Icarus 280 (2016) 308–314

Contents lists available at ScienceDirect

Icarus

journal homepage: www.elsevier.com/locate/icarus

Results of a hubble space telescope search for natural satellites of dwarf planet 1 ceres

Benjamin E. DeMario[a,*], Britney E. Schmidt[a], Max J. Mutchler[b], Jian-Yang Li[c], Lucy A. McFadden[d], Brian J. McLean[b], Christopher T. Russell[e]

[a] School of Earth and Atmospheric Sciences, Georgia Institute of Technology, 311 Ferst Drive Atlanta, GA 30312, USA
[b] Space Telescope Science Institute, 3700 San Martin Drive, Baltimore, MD 21218, USA
[c] Planetary Science Institute, 1700 East Fort Lowell, Suite 106, Tucson, AZ 85719-2395, USA
[d] Goddard Space Flight Center, 8800 Greenbelt Rd, Greenbelt, MD 20771, USA
[e] Department of Earth, Planetary, and Space Sciences, University of California, Los Angeles 595 Charles Young Drive East, Box 951567, Los Angeles, CA 90095-1567, USA

ARTICLE INFO

Article history:
Received 1 January 2016
Revised 6 July 2016
Accepted 7 July 2016
Available online 14 July 2016

Keywords:
Asteroid Ceres
Satellites of asteroids
Hubble Space Telescope observations

ABSTRACT

In order to prepare for the arrival of the Dawn spacecraft at Ceres, a search for satellites was undertaken by the Hubble Space Telescope (HST) to enhance the mission science return and to ensure spacecraft safety. Previous satellite searches from ground-based telescopes have detected no satellites within Ceres' Hill sphere down to a size of 3 km (Gehrels et al. 1987) and early HST investigations searched to a limit of 1–2 km (Bieryla et al. 2011). The Wide Field Camera 3 (WFC3) on board the HST was used to image Ceres between 14 April–28 April 2014. These images cover approximately the inner third of Ceres' Hill sphere, where the Hill sphere is the region surrounding Ceres where stable satellite orbits are possible. We performed a deep search for possible companions orbiting Ceres. No natural companions were located down to a diameter of 48 m, over most of the Hill sphere to a distance of 205,000 km (434 Ceres radii) from the surface of Ceres. It was impossible to search all the way to the surface of Ceres because of scattered light, but at a distance of 2865 km (five Ceres radii), the search limit was determined to be 925 m.

1. Introduction

Ceres is the first object that was discovered in the asteroid belt between Mars and Jupiter. In many ways, it is a unique object, being the largest object, and the only one to assume a hydrostatic shape in the asteroid belt. It also possesses the spectral signature of phyllosilicates, organics, ammoniated species, and carbonates on its surface (Rivkin et al. 2002, Milliken et al. 2009, DeSanctis et al. 2015). In 2006, the IAU re-categorized Ceres to 'Dwarf Planet' alongside other objects such as Pluto and Eris. Dawn arrived at Ceres in March 2015. The first exploration of Ceres by the Dawn mission has provided opportunities to better understand Ceres' history, as well as the evolution of the early Solar System (Russell et al. 2007). With Dawn entering orbit with only two reaction wheels, serious constraints are placed on pointing, limiting the dedicated satellite search and the possibility of observations of such a satellite if one were detected (Polanskey et al. 2014). Thus, with the approach of Dawn imminent, we undertook a search for satellites of Ceres using the Hubble Space Telescope in April 2014.

Over 270 asteroids, even small ones, are known to have Moons or be binary (Johnston 2016). The first asteroid with a Moon was observed by the Galileo spacecraft in 1993 as it passed the 16 km S-class asteroid 243 Ida, revealing its small Moon Dactyl at a distance of 90 km (Chapman et al. 1995). There are 58 known satellites of near-Earth asteroids, 117 known around main belt asteroids, and at least 95 around minor planets elsewhere in the Solar System. Asteroid satellites can be formed by a number of processes, including impact ejection, impact disruption, and reaccretion (Weidenschilling 1980, Merline et al. 2002). Notably, the Yarkovsky-O'Keefe-Radzievskii-Paddack (YORP) effect can cause elongated or odd-shaped asteroids that pass near the Sun to significantly increase in rotation speed (Lowry et al. 2007). As an asteroid releases heat as thermal energy, this process is also able to add angular momentum, causing an asteroid's rotation rate to change to a degree that fission may occur (Pravec et al. 2010). Ceres' spin rate, with a rotational period of nine hours, is too slow to fission material. However, with its large cross section, it has certainly experienced impact events that could liberate material to

* Corresponding author.
E-mail addresses: bennygleepdiddly@gmail.com, bdemario3@gatech.edu (B.E. DeMario), britneys@eas.gatech.edu (B.E. Schmidt).

http://dx.doi.org/10.1016/j.icarus.2016.07.005
0019-1035/

form Moons. Its hydrostatic shape with relatively subdued topography should allow for stable satellite orbits (Scheeres et al. 1996). However, the large asteroid 4 Vesta, which is about half the diameter of Ceres and is thought to have formed in a similar way, possesses no satellites down to a radius of 3–6 m (Memarsadeghi et al. 2012, McFadden et al. 2015). Either result would be of scientific value. Beyond the novelty of detecting a satellite, observations of a Moon could help constrain Ceres' history and composition. Differently from Vesta (Zappala et al. 1995), no meteorite has been identified as a spectral match for Ceres. This has been interpreted as one of many indications that Ceres is ice rich (Russell et al. 2007, Rivkin et al. 2014), thus discovery of a Moon could shed light on this hypothesis.

Satellite searches are common practice for small bodies, especially those with approaching spacecraft (e.g. Chapman et al. 2002). Weaver et al. (2006) and Showalter et al. (2011, 2012) discovered four additional satellites surrounding the Pluto-Charon system using the Hubble Space Telescope's cameras. In addition, McFadden et al. (2012) used similar Hubble imaging techniques to study the asteroid Vesta's neighborhood prior to Dawn's arrival. Their investigation concluded that no satellites existed that were larger than 22 +/- 2 m radius, a result which was confirmed and improved upon to 3–6 m when Dawn arrived at Vesta (Memarsadeghi et al. 2012, McFadden et al. 2015). Previously, Bieryla et al. (2011) searched for Moons around Ceres using the Hubble Space Telescope and found none down to a size limit of about 1 km. Ground-based observations of Ceres were also utilized to conduct a deep Moon search, returning no detections of satellites down to 2 km within Ceres' full Hill sphere (Bieryla et al. 2011).

2. Methods

2.1. Hubble Space Telescope Satellite Search

We used the Hubble Space Telescope's Ultraviolet and Visible Light Wide Field Camera 3 (UVIS WFC3), a third-generation HST instrument that provides the highest spatial resolution of any of its instruments at 0.04″/pixel. Unaffected by atmospheric variability that plagues ground-based telescopes, HST is ideal for the satellite search because of its extremely stable thermal environment, well-characterized detectors, and high sensitivity. We used an approach similar to satellite investigations that have been conducted for Vesta, Ceres, and Pallas using HST (McFadden et al. 2012, Bieryla et al. 2011, Schmidt et al. 2009). The goal of the study was to exceed the limits of previous satellite searches that were complete to object sizes of 1–2 km within the full Hill sphere. The 2006 HST study (Li et al. 2006) did not include many deep exposures required to detect satellites smaller than about 1 km since its focus was on Ceres itself, not potential satellites. The ground-based search was limited to observing far from Ceres due to atmospheric seeing limitations. Thus, we chose an approach that combined several techniques to draw out any possible satellites hidden by previous work.

We observed during four 96-min HST orbits between April 14 to 28, 2014 (HST program 13,503, PI Britney Schmidt). These observations occurred when Ceres was at 5° phase angle and reached an angular size of 0.82″. We obtained deep exposures with the WFC3 in the UVIS F350LP filter (long-pass, visible 300–800 nm). The observations were intentionally spaced at different intervals of 1 day, 5 days, and 8 days between orbits to minimize aliasing with any possible satellite orbital periods. We did not specify the orientation of the spacecraft, and so obtained a random distribution of the placement of the diffraction spikes to avoid obscuring satellites in a systematic way. The observations included short 0.5 s and 5 s exposures, reading out small subarrays to search near Ceres for close-in satellites missed by previous surveys (with less obscuration from saturation and scattered light). There were also mid- and long-exposures of 30, 120 and 180 s in duration where Ceres was intentionally overexposed to search the greater part of Ceres' Hill sphere (using full CCD readouts) for objects much smaller in size and/or further away from Ceres (which is significantly saturated in the long exposures). Details of the observations are shown in Table 1.

Table 1
Summary of exposures taken over the course of four HST orbits. All images were taken with the WFC3 camera in the F350LP filter.

Hubble Space Telescope observations of Ceres		
	Date and Time (UTC)	Exposure times
Orbit 1	14 April 2014, 16:04 – 16:39	120 s x 2, 30 s x 4, 5 s x 4, 0.5 s x 6
Orbit 2	15 April 2014, 14:22 – 14:59	120 s x 2, 30 s x 4, 5 s x 4, 0.5 s x 6
Orbit 3	20 April 2014, 12:18 – 12:52	180 s x 2, 30 s x 2, 5 s x 4, 0.5 s x 5
Orbit 4	28 April 2014, 13:01 – 13:37	180 s x 2, 30 s x 2, 5 s x 4, 0.5 s x 5

2.2. Data processing and analysis

2.2.1. Image products

Starting with calibrated WFC3 images retrieved from the Mikulski Archive for Space Telescopes (MAST), we further distortion-corrected, aligned, and combined the images to produce three different data products. Each image was 'drizzled', and then the images were aligned by placing the intersection of diffraction spikes, which corresponds with the center of Ceres, at the direct center of each image. Finally, the exposed portions of the images were rotated to place north up. The first product, a sum image, is simply a linear addition of multiple images, each with the same exposure time, taken during a single orbit. The second product, 'combine', is a clean image obtained by taking the median of each corresponding pixel in multiple images, and using that as the value to the corresponding pixel in the output image. In the case where there are only two such images per orbit, as is the case for the 120-s and 180-s exposures, this filter simply becomes a mean-filter, which acts to slightly suppress cosmic rays. For the third product, we applied unsharp-masking, a digital enhancement process in which a Gaussian convolution of the original was subtracted from the original image. We apply this to the clean, combined images in order to create an image product with a flatter dynamic range making it easier to identify faint candidate satellites. These processing methods are valuable for initial investigation because they remove a large number of obvious artifacts and stars while still allowing a thorough search. However, these methods can remove candidate objects from the data, so verification involves a careful inspection of these data products to rule out artifacts and identify candidate objects. We searched by comparing (blinking) the combined and single images to search for satellites using SAOImage DS9. In the final phase of the investigation, we added artificial Gaussian point-spread functions at different locations into the original data to simulate detectable satellites at a range of sizes. Based on whether or not these artificially added objects could be detected by the methods of the original search, a limitation on search magnitude could be set. In Fig. 1 we show an example HST search image, a 'sum' of two 180-s exposures, where Ceres is overexposed and placed in the center of the image. In Fig. 2 we show the same two 180-s exposures, as they appear when processed with 'combine' and 'unsharp', respectively.

2.2.2. Search methodology

In order to compare the search results of the processed images with potential physical results, we investigated the expected motion of a true satellite between frames. The Hill sphere is a region

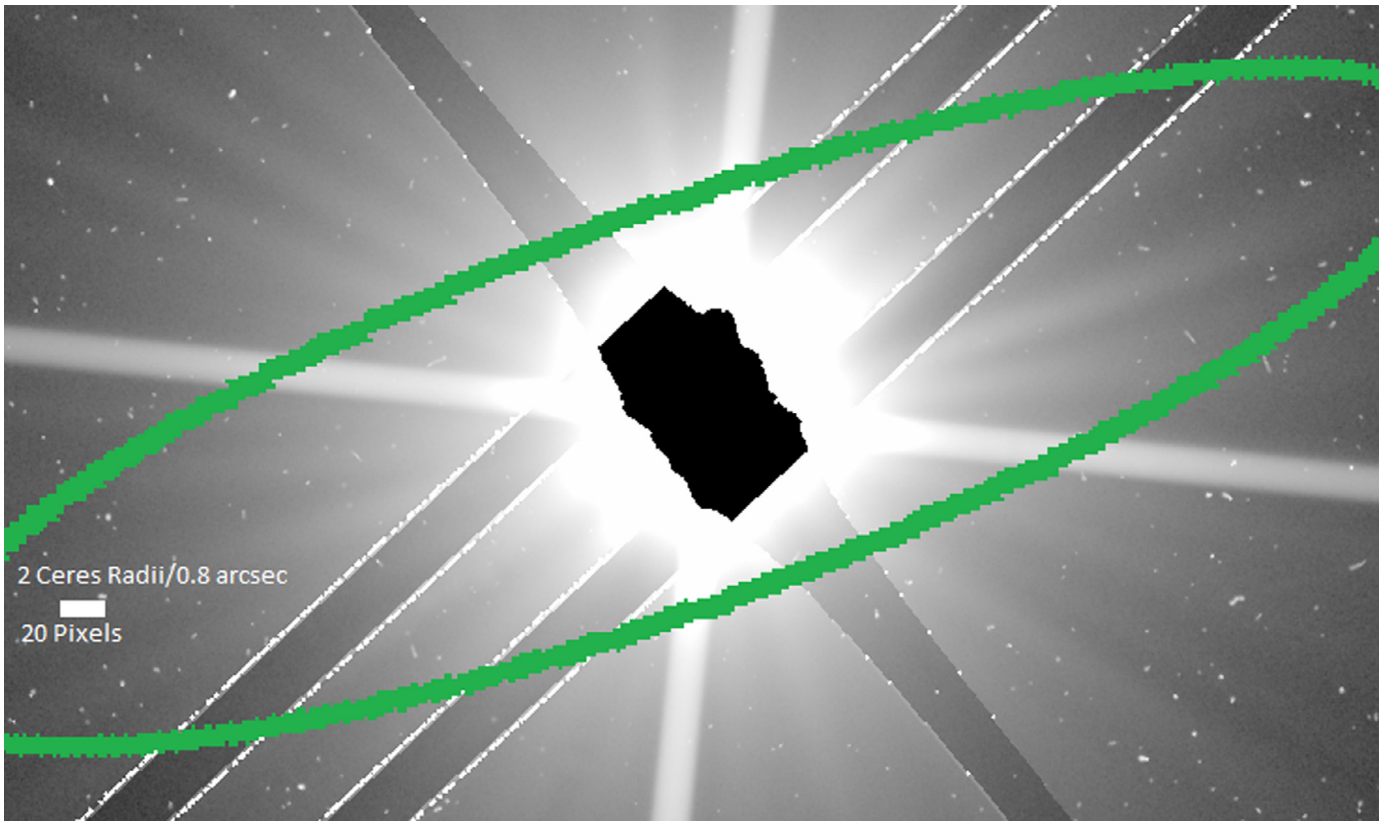

Fig. 1. Small central section of a sum of two 180-s (heavily overexposed and saturated) images of Ceres taken by the HST using the WFC3 camera in the UVIS F350LP filter on 20 April 2014, revealing the many artifacts obscuring our search. At this phase of processing, no steps were taken to remove cosmic rays from the images. The images have been rotated to place north up. In each orbit the diffraction spikes occur in different points. Here, Ceres would be about 20 pixels across and is in the very center of the image, which contains only saturated pixels that were rejected. The dark region in the center is the overexposed area recorded as black in the image because it was masked out during processing. There are cross-spikes around Ceres as a result of diffraction caused by the spider holding the optics of the telescope. We also note the approximately lower-left-to-upper-right CCD chip gaps, and the approximately upper-left-to-lower-right residuals from the saturation and bleeding of Ceres. The large green ellipse represents a circle approximately in the equatorial plane of Ceres, where the upper half of the ellipse tilts toward the viewer and the lower half tilts away. This is the most likely orbital path for a satellite with a greatest separation of ~438 pixels, which corresponds to a semi-major axis of 20,590 km. In this particular image, there are various cosmic rays, star trails, and camera artifacts obscuring the background that is then carefully searched for objects.

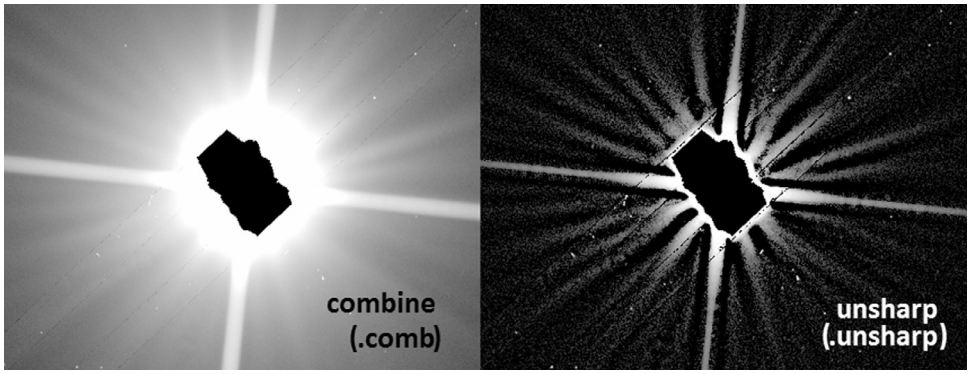

Fig. 2. The same two 180-s exposures that made up Fig. 1, processed with 'combine' and 'unsharp' methods, respectively. Of note is the suppression of the chip gaps and residuals due to the mean-filtering. In addition, the 'unsharp' method has removed a Gaussian model of the stray light surrounding Ceres, thus flattening the dynamic range of the image to be studied.

of space surrounding a body where its gravitational influence exceeds the perturbing forces from other bodies such as the Sun. We would expect any satellites present around Ceres to be present in the Hill sphere, which has a size of 434 Ceres radii (205,000 km, or 180″). Moreover, over a long period of time, we would expect solar radiation, oblateness in the shape of Ceres, and perturbations from objects in the plane of the ecliptic to move satellite orbits towards perfect circles in the plane of Ceres' equator (Hamilton and Burns, 1992). Thus, we only need to search the Hill sphere for satellites since we do not expect them to be seen elsewhere.

Additionally, a natural satellite would move in a Keplerian orbit, which would likely be reasonably circular owing to the factors above, and in line with Ceres' equator (Hamilton and Burns 1992), though this was not a strict limitation of the search. By using the known mass of Ceres of 9.39×10^{20} kg

(Standish and Hellings 1989), we can calculate the lengths of orbits in the Hill sphere to predict how a satellite at a given distance from Ceres would appear to move. A satellite orbiting 3 Ceres radii (1419 km) from the center of Ceres, near the Roche Limit, would complete an orbit in 12 h, whereas one at the extreme outer boundary of the Hill sphere at 434 Ceres radii (205,000 km) would take about 2.39 years to complete an orbit. As an example for an object likely to be detected by the actual search, we must make use of the fact that one pixel of 0.04″ corresponds to 47 km at the distance of Ceres. 400 pixels from the center of Ceres is approximately the point where stray light from Ceres becomes a consideration. A satellite whose greatest separation occurs 400 pixels from the center of Ceres would have a semi-major axis of 18,800 km, and would complete an orbit in 24.2 days. Thus, this object would move around its orbit at a rate of just over one half degree per hour. If this object were moving at a 45° angle 'in' or 'out' with respect the image plane, which would be the case at four points in the orbit, it would be seen travel across the image plane at three pixels per hour, or a total of 2.94″ (73 pixels) per day. These numbers will necessarily differ for satellites located nearer to or further from Ceres, although these calculations give us an expectation for about how quickly a true satellite should move. The rate of motion in pixels/day varies as the -1/2 power of the satellite's semi-major axis. At the edge of the Hill Sphere, we expect a rate of motion of about 22 pixels per day.

To seek out candidate objects, the images were split into smaller groups of images to be compared. Initially, the search was focused on the longest exposures – i.e. the outer regions of the two 120 s or 180 s exposures from each orbit were respectively blinked against each other. These exposures represent the deepest exposures of Ceres taken by HST, and as such would have the greatest likelihood of detecting satellites. These images contain approximately the inner 1/3 of the Hill sphere of Ceres, meaning any objects found in these images are likely to have stable orbits. However, if the objects were too close to Ceres, the scattered light contributed by the proximity of Ceres would have rendered them impossible to detect. The 180-s exposures contained a large number of candidate objects, because of the large number of cosmic rays and other artifacts that accumulated over the exposure duration. Because these exposures were taken on the order of 30 min apart from each other, true satellites should display relatively little motion in between these exposures (only on the order of a pixel). If an object appeared within several pixels over the course of the two longest exposures in an orbit, long exposures from another orbit were then blinked to try and find the object in a frame taken days later. If it could be found in a position that would be consistent with Keplerian motion, an attempt was then made to fit an orbit to the candidate object and find it in more exposures.

Following the analysis of data from all 180-s and 120-s exposures, attention turned to the shorter 30-s exposures, which were also analyzed by blinking images within the same orbit, and then looking for any candidate detection from other orbits that showed limited or no relative motion within that orbit or that could have been obscured by a diffraction spike in the other images. This exposure length allowed the area closer to Ceres to be observed with less noise from Ceres. We thus increased the chance of finding any satellites orbiting much closer to Ceres than would be detectable in the longer exposures or to be seen from the ground by focusing search efforts on the area closer to Ceres itself. Occasionally, the 30-s exposures were blinked against the longer exposures, although this was not preferred because the shorter exposures utilized subarray readouts, and the different image dimensions made it difficult to blink the images.

Finally, shorter 0.5-s and 5-s exposures provided the opportunity to search for larger objects close to Ceres (and only small CCD subarrays were read out). These images were studied well because of the many circumstances that may hide Moons. It is distinctly possible that cosmic rays, diffraction spikes, and poor viewing angles may have hidden Moons from all previous exposures. By studying data taken at different time intervals and different exposure times, the likelihood of these objects being missed is minimized.

Ultimately, the longest exposures proved most useful. There was a significant difference in the amount of stray light, particularly very close to Ceres. However, not many candidate objects were identified in the shorter exposures, because the limiting magnitude closer to Ceres was much lower.

2.2.3. Candidate criteria

Candidate objects were identified based on the following set of criteria that would distinguish them from noise or cosmic rays. Candidates: (1) have Gaussian shaped point-spread brightness functions, (2) did not saturate the detector (generally indicative of cosmic ray interference), and (3) appeared in more than one of the unedited HST exposures as well as the processed images. After identifying candidate objects based on their appearance, their motion must be found to be consistent with Keplerian motion around Ceres to potentially be a real object. The locations of objects fitting the first three criteria were recorded so that further analysis could be done to either confirm or rule out these objects by attempting to fit a Keplerian orbit to the candidate object. A simple 'A, B, C' rating scale was devised to gauge how convincing an object appearing in the data was. A 'C' object was one that was likely an artifact, because it did not possess the expected appearance of a satellite (i.e. not having a smooth Gaussian point-spread function) and/or was only visible in one image. 'B' objects represent the vast majority of objects recorded in the data – they possess the approximate appearance of a satellite, were visible in more than one image, and some were moving in a way that could be compared to that of an actual satellite. Only one object observed was given an 'A' rating – which denoted an object that had the exact appearance of a small satellite, was visible in multiple images across multiple orbits, and moved in a way that would have been expected of a satellite undergoing Keplerian motion. In Fig. 3, we show an example of 'A', 'B', and 'C' objects. The list of candidates is included in Table 2, with pixel coordinates (x, y) in our processed images.

Stellar contamination was relatively unimportant. At the time of observation, Ceres was located in the constellation of Virgo in a region far out of the galactic plane, so the number of visible stars was relatively minimal. Indeed, not many bright stars were identified in the images. Ceres' motion relative to the background stars was about 1′/h, so the motion of background stars was clearly identifiable in the exposures of 30 s or longer. Thus, most contamination in the images was due to cosmic rays or shot noise.

2.2.4. Candidate detections

The positions and ratings for candidate objects were recorded for further study. At the end of the observations, thirteen candidate objects were given ratings of 'A' or 'B' from 180-s exposures, eight candidate objects from 120-s exposures, and twelve candidate objects from 30-s exposures. No likely candidate objects were identified in the short exposures of 5 s and 0.5 s, although the data were comprehensively searched.

An immediate and striking observation is that the vast majority of candidate objects originated from the longer exposures of 180 and 120 s. This is partially due to the deeper exposures setting the limiting magnitude of search substantially higher in these exposures. In addition, some candidate objects were artifacts from the less complete cosmic ray rejection and the higher level of accumulated shot noise in these images. For example, the single 'A' object was likely the remnant of such a series of artifacts. Conversely, we found almost no convincing objects in the shorter exposures

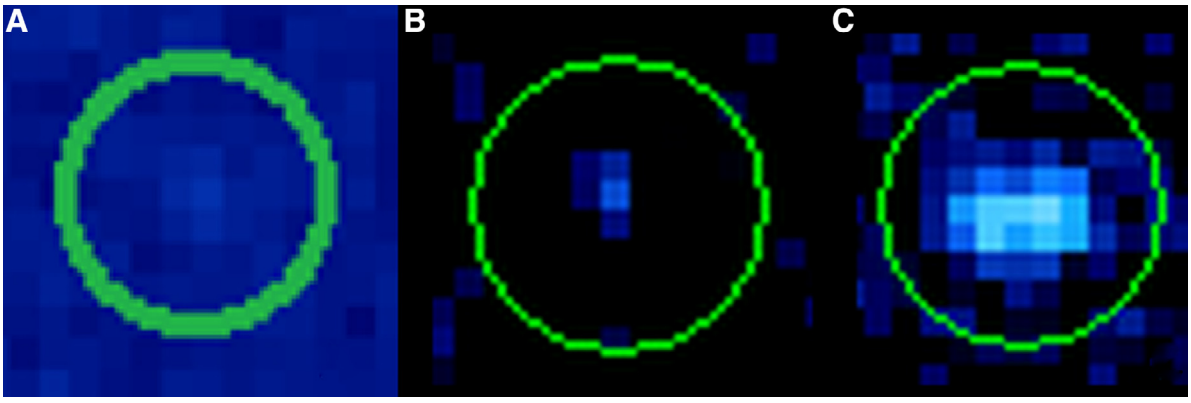

Fig. 3. Left to right, we show examples of objects rated 'A', 'B', and 'C' respectively in WFC3 images (scale 0.04″/pixel). There was only one 'A' object in the HST data – it took on a similar appearance in all images and moved slowly through the images in a way that was consistent with Keplerian motion. The 'B' object has the appearance of a satellite, possessing the expected Gaussian point-spread function, but needed to be further studied to determine if its motion through images was characteristic of Keplerian motion. The 'C' object, however, has a distinct 'double' shape indicating that it is likely the intersection of two cosmic rays or other artifacts. Based on this characteristic the 'C' object could be quickly ruled out.

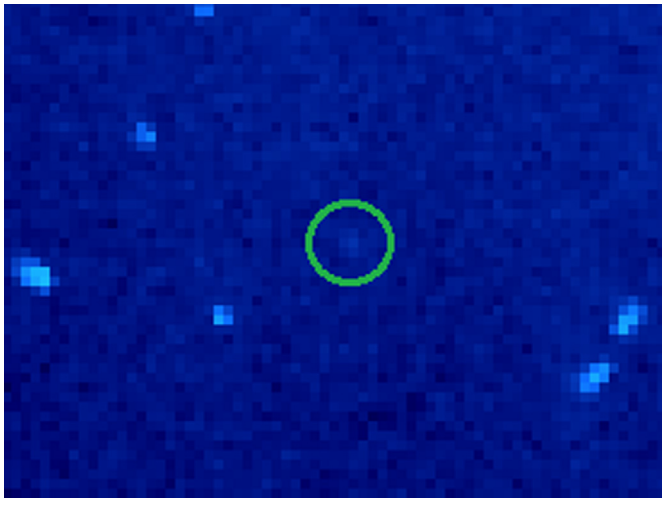

Fig. 4. Artificial object of apparent magnitude 28.4 added to long-exposure Ceres data as an artificial object. This was one of the dimmest objects that could be identified as such in the search.

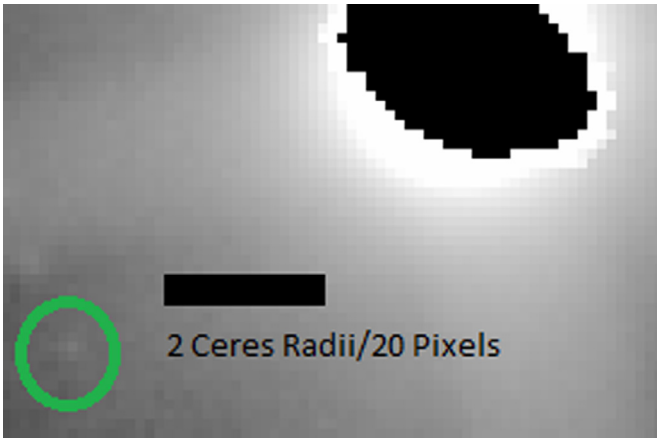

Fig. 5. Artificial object of apparent magnitude 22.0 seen within 50 pixels of Ceres in a 0.5-s exposure. The black region is the saturated region. This was the dimmest artificial object detected near Ceres and thus places an upper limit on the sizes of objects that may exist closest to Ceres.

Table 2
Candidate objects noted as part of the satellite search. Most important is the object found in the image from April 14th which is marked 'A'. Objects of classification 'C' were not recorded unless there was another important quality of the object, such as it being close to a diffraction spike. Very few notable objects were found in 5-s and 0.5-s exposures, likely because of the much deeper sensitivity of the longer exposures. The '+' and '-' designations were given to objects that intuitively seemed more or less likely to be a real object than other objects given the same letter classification.

Image filename	X	y	#
ceres_wfc3_f350lp_140,414_120s	3430	2925	B-
	2642	3743	B
	3304	3725	B
	3192	4005	B-
	2293	3297	B
ceres_wfc3_f350lp_140,415_120s	3485	3398	B
	3511	3324	B
	2889	3565	B
ceres_wfc3_f350lp_140,420_180s	2892	3021	B
	2973	3037	B
	3054	2844	B
	3176	2915	B
	2845	3003	B
	2852	3072	B
	2738	3156	B
	2008	3596	B
ceres_wfc3_f350lp_140,428_180s	1376	2757	B
	1737	2737	B-
	3394	1825	B
	990	1601	C
	3553	2527	B-
ceres_wfc3_f350lp_140,420_30s	3236	2920	B-
	3289	3025	B
ceres_wfc3_f350lp_140414a_30s	971	787	C
	1086	756	A
	1138	911	B-
	1099	892	B
	498	1015	C+
	329	829	B
	1051	728	B-
	1118	770	B
ceres_wfc3_f350lp_140414b_30s	956	981	C+
	1113	775	B

of 5 and 0.5 s. As before, this is due to the far lower limiting magnitude in these short exposures. Finally, the shorter exposures were largely focused on the area closest to Ceres with the most stray light. Because the area to be searched most thoroughly in the short exposures is far smaller than that to be searched in the long

exposures, more candidate objects are to be expected in the longer exposures due to searching a much larger area of the image more sensitively.

After all of the images had been thoroughly studied, all 'A' and 'B' objects were re-evaluated to assess whether or not those detections could be real satellites. During the initial identification of candidate objects, we assessed their motion by blinking images back and forth that were taken at the beginning and end of an orbit. For this secondary evaluation, the area near the candidate object was studied during a different orbit from several days before or after. Many candidate objects were thus eliminated because they could not be found in any nearby position in a different orbit. Additionally, the angular motion of a satellite moving in a circular orbit should be constant; for example, if an object moves by three degrees in a one hour time period, it needs to move by six degrees in a two hour time period. Based on this idea, it is possible to calculate where a candidate object should be in an earlier or later orbit, if its position in two or more orbits are known. Moreover, the one object which was recorded as 'A' class was ruled out. The object was originally seen in all of the exposures on 14 April, and only moved by a few pixels between the two 180-s exposures on that day, which were taken at the beginning and end of the observations to allow for the greatest possible amount of satellite motion. Moreover, in the orbit on 15 April one day later, it was seen about sixty pixels away in the 30-s exposures. In addition, the object did not move in a way that could be expected of a near-Earth asteroid, a star, or a main-belt asteroid. A number of possible circular orbits centered on Ceres were fit to the points allowing the prediction of the object's position in other orbits. However, it could not be located in any predicted position in the orbits on 20 April or 28 April. Thus, it was determined that the object was likely a series of artifacts, which coincidentally happened to appear similarly in multiple exposures. After searching the data for objects, nothing was found that matched the expected appearance of a natural satellite.

3. Results and discussion

While we did not find any satellites, we can put limits on the brightness and size of potential satellites. We devised a means to test the limiting magnitude of the search and hence to set limits on the size of satellites that were detectable. Artificial objects of known magnitude were inserted into the data, some of which mimic Moons and some of which mimic background objects, and the newly created simulated images were studied. Two different observers searched for the objects inserted in the data. Based on whether or not the observers could detect artificial objects of known magnitude, a limit on the brightness, and hence the size, of satellites was set, assuming the artificial objects have the same geometric albedo as Ceres.

The artificial objects were added to the data using a MATLAB program. Using the known photometric zeropoint of the UVIS F350LP filter being used, the program can simulate the appearance of objects of a specific apparent magnitude. The program added Gaussian point-spread functions on a 'per-orbit basis' to the data. A randomly generated number from 1–20 was chosen to determine how many artificial objects to add. The objects were added to the data in reasonable Keplerian orbit locations within the image with a range of brightnesses that could be specified. Once Gaussians of a known apparent magnitude were added to the data, the images were then searched again using the same methods of the original search. Because a true satellite would not move appreciably over the course of a 35-min observing window unless it were quite close to Ceres, blinking between these modified images within an orbit provides an effective way of determining how bright a satellite must be to be seen above the shot noise variation between images during the original search. Artificial objects located in this search were found only based on blinking them with another image that had a different shot noise pattern. This search methodology is most similar to the necessary condition for an object to have been assigned an 'A' or 'B' rating during the original search. The search does not address the ability to fit a Keplerian orbit to a candidate object that has been detected, which is independent of the magnitude of the detected objects.

In addition to the search itself, an attempt was made to quantify the effect of stray light on the limiting magnitude in different regions of the image. To do this, the image was divided into ring-shaped regions based on distance from the center of Ceres. Keeping in mind that Ceres spans about twenty pixels across in these images, the regions were decided to be: more than 400 pixels away from Ceres, 200–400 pixels away, 100–200 pixels away, and 50–100 pixels away. These regimes approximately correspond to the regions where the 180-s, 30-s, 5-s, and 0.5-s exposures were most useful in the original search, respectively. The program adding artificial objects was restricted to place objects into these regions, and the images were again searched.

The brightnesses of objects that were found were recorded to the nearest 0.1 magnitude. We made use of a 'double blind' approach where objects were added to the data, but the number of objects and the locations of the objects were not printed out until after an effort was made to find all of the objects. All possible artificial objects were identified, given a letter rating from 'A' to 'C', and studied for follow-up. This approach has the advantage that it best mimics the original process that was employed while searching the images for satellites – the same program was used to switch between the original files and the files with the artificial objects, and the positions of candidate artificial objects were recorded in the same way. In addition, the extra time spent searching the original images reduces the possibility that any objects were missed during the original satellite search.

We completed the search of images of all exposure lengths for both real and implanted objects over a range of magnitudes. No natural satellites were detected during any phase of the search. Based on the detected implanted objects, we determined that the limiting magnitude of the search was 28.4, as this represents the dimmest objects where all artificial objects were correctly identified in the data. Using the distance from Earth to Ceres (1.63 AU) and the distance from the Sun to Ceres (2.62 AU) as determined from ephemerides, we concluded that the absolute magnitude of detectable objects was 24.8. Assuming these objects have Ceres' published albedo of 0.09 (Li et al. 2006), this brightness would correspond to objects that are 48 m in diameter. If the albedo of such an object happens to differ from that of Ceres, the size of the object will differ by a factor of sqrt(0.09/albedo).

In regions of the image closer to Ceres, the limiting magnitude was smaller due to scattered light from Ceres. In a worst-case scenario, however, an object at apparent magnitude 22.0 was still visible even when less than five Ceres radii away from the surface. This magnitude corresponds to an absolute magnitude of 18.4, and hence a satellite diameter of 925 m.

The determined limiting magnitudes of search for the different ring-shaped regions around Ceres are summarized in Table 3.

Although the field of view of the HST images only encompasses the inner third of the Hill sphere, the irregular cadence of the observing runs across April 2014 and the variety of image exposures, coupled with the increased likeliness that satellites will orbit the equator of Ceres mean that most satellites would be detected out to the edge of the Hill sphere except those in extreme orbits. The method of searching for objects in HST data with SAOImage DS9 by switching images rapidly provides the maximum sensitivity that may be attained with current capabilities outside of in-situ spacecraft data.

Table 3
Limitations of search to the nearest 0.1 magnitude for artificial objects placed in ring-shaped regions of HST data. A smooth, approximately logarithmic function giving the radial dependence of satellite diameter may be interpolated if desired.

Limiting magnitude of search versus distance from Ceres			
Distance from Ceres (pixels)	Visual limiting magnitude	Corresponding satellite diameter with albedo of Ceres (meters)	Exposure time with faintest limiting magnitude
400+	28.4	48	180 s, 120 s
200–400	26.7	106	30s
100–200	24.7	266	5s
50–100	22.0	925	0.5s

4. Conclusions

We conclude that, to a radius of roughly 5 Ceres radii (2865 km), Ceres does not possess any satellites larger than 925 m in diameter. In addition, Ceres does not possess any satellites larger than 48 m diameter out to the edge of its Hill sphere (205,000 km). Via the use of HST's WFC3, plus the use of multiple exposure times, irregular cadence of observing windows, as well as the additional checks provided by the artificial object search, we have carried out a complete analysis of the possibility of satellites around Ceres. Our search allows us to place these lower limits as our detection limits. Thus, this study represents the most complete survey for satellites that has been undertaken for Ceres, and is the most sensitive study achievable outside of Dawn's survey.

As a follow-up to this study, other researchers making use of images captured from the Dawn spacecraft at Ceres will place additional limits on the sizes of any satellites around Ceres. Similar methods to those reported here can be used to analyze the Dawn spacecraft data. Such a study will place further refinements on the size of satellites around Ceres, as well as detect any satellites that may be too faint to detect with HST.

The absence of a satellite is not a surprise based on current formation models for asteroid satellites. Although objects of comparable size in the Kuiper Belt such as Pluto and Eris each have natural satellites, and many very small asteroids have companions, the two largest main-belt asteroids Ceres and Vesta do not have any companions detectable with current capabilities. The fact that both Ceres and Vesta lack satellites, whereas the dwarf planets in the Kuiper Belt do host satellites, supports the idea that satellite formation mechanisms in the two different belts are fundamentally different.

Acknowledgments

This work was supported by Space Telescope Science Institute GO 13503, PI Schmidt. The authors express thanks for the support of STSCI and the Dawn Mission Team.

References

Bieryla, A., Parker, J.W., Young, E.F., et al., 2011. A Search for Satellites around Ceres. Astron. J. 141 (6), 197.
Chapman, C.R., Veverka, J., Thomas, P.C., et al., 1995. Discovery and physical properties of Dactyl, a satellite of asteroid 243 Ida. Nature 374 (6525), 783–784.
Chapman, C.R., Merline, W.J., Thomas, P.C., et al., 2002. Impact history of Eros: Craters and boulders. Icarus 155 (1), 104–118.
De Sanctis, M.C., Ammannito, E., Raponi, A., et al., 2015. Ammoniated phyllosilicates with a likely outer Solar System origin on (1) Ceres. Nature 528, 241–244.
Gehrels, T., Drummond, J.D., Levenson, N.A., 1987. The absence of satellites of asteroids. Icarus 70 (2), 257–263.
Hamilton, D.P., Burns, J.A., 1992. Orbital stability zones about asteroids: II. The destabilizing effects of eccentric orbits and of solar radiation. Icarus 96 (1), 43–64.
Johnston, W.R., 2016. Asteroids with Satellites. Retrieved March 15, 2016, from http://www.johnstonsarchive.net/astro/asteroidmoons.html. (accessed 15.03.16.).
Li, J.Y., McFadden, L.A., Parker, J.W., et al., 2006. Photometric analysis of 1 Ceres and surface mapping from HST observations. Icarus 182 (1), 143–160.
Lowry, S.C., Fitzsimmons, A., Pravec, P., et al., 2007. Direct detection of the asteroidal YORP effect. Science 316 (5822), 272–274.
McFadden, L.A., Bastien, F.A., Mutchler, M., et al., 2012. Upper limits on the size of satellites of Asteroid (4) Vesta from 2007 Hubble Space Telescope observations. Icarus 220 (2), 305–310.
McFadden, L.A., Skillman, D.R., Memarsadeghi, N., et al., 2015. Vesta's missing Moons: Comprehensive search for natural satellites of Vesta by the Dawn Spacecraft. http://dx.doi.org/10.1016/j.icarus.2015.04.038.
Memarsadeghi, N., McFadden, L.A., Skillman, D.R., et al. (2012, February). Moon search algorithms for NASA's dawn mission to asteroid Vesta. In Proceedings of IS&T/SPIE Electronic Imaging. International Society for Optics and Photonics. pp. (pp. 82960H-82960H. doi:10.1117/12.915564.
Merline, W.J., Weidenschilling, S.J., Durda, D.D., et al., 2002. Asteroids do have satellites. Asteroids III 1, 289–312.
Milliken, R.E., Rivkin, A.S., 2009. Brucite and carbonate assemblages from altered olivine-rich materials on Ceres. Nat. Geosci. 2, 258–261.
Polanskey, C.A., Joy, S.P., Raymond, C.A., Rayman, M.D., 2014. Architecting the Dawn Ceres Science Plan. Space Operations, Pasadena, CA.
Pravec, P., Vokrouhlický, D., Polishook, D., et al., 2010. Formation of asteroid pairs by rotational fission. Nature 466 (7310), 1085–1088.
Rivkin, A.S., Howell, E.S., Vilas, F., Lebofsky, L.A., 2002. Hydrated Minerals on Asteroids: The Astronomical Record. In: Asteroids III University of Arizona Press.
Rivkin, A.S., Asphaug, E., Bottke, W.F., 2014. The case of the missing Ceres family. Icarus 243, 429–439.
Russell, C.T., Capaccioni, F., Coradini, A., et al., 2007. Dawn mission to Vesta and Ceres. Earth Moon Planets 101 (1-2), 65–91.
Scheeres, D.J., Ostro, S.J., Hudson, R.S., et al., 1996. Orbits close to asteroid 4769 Castalia. Icarus 121 (1), 67–87.
Schmidt, B.E., Thomas, P.C., Bauer, J.M., et al., 2009. The shape and surface variation of 2 Pallas from the Hubble Space Telescope. Science 326 (5950), 275–278.
Showalter, M.R., Hamilton, D.P., Stern, S.A., et al., 2011. New satellite of (134340) Pluto: S/2011 (134340) 1. *International Astronomical Union Circular*, *9221*, 1.
Showalter, M.R., Weaver, H.A., Stern, S.A., et al., (2012). New satellite of (134340) Pluto: S/2012 (134340) 1. *International Astronomical Union Circular*, *9253*, 1.
Standish, E.M., Hellings, R.W., 1989. A determination of the masses of Ceres, Pallas, and Vesta from their perturbations upon the orbit of Mars. Icarus 80 (2), 326–333.
Weaver, H.A., Stern, S.A., Mutchler, M.J., et al., 2006. Discovery of two new satellites of Pluto. Nature 439 (7079), 943–945.
Weidenschilling, S.J., 1980. Hektor: Nature and origin of a binary asteroid. Icarus 44 (3), 807–809.
Zappala, V., Bendjoya, P., Cellino, A., et al., 1995. Asteroid families: Search of a 12,487-asteroid sample using two different clustering techniques. Icarus 116 (2), 291–314.